effect of 8-kbar pressure on the σ of the Red Sea olivine is equivalent to less than ±5°C temperature change (within the 95% confidence limit) between 1270° and 1440°C.

The A_x and σ_x given in Table 1 for σ in the Red Sea olivine may be compared with those from other studies on σ in olivine single crystals (Table 2). Because of uncertainties associated with grain boundaries, degree of compaction, impurity levels, and oxidation state of the cations in the various samples, most of the σ data on natural or synthetic monomineralic aggregates are difficult to interpret. Also, since most previous studies of σ of olivine single crystals have been performed on relatively highly conductive, partially oxidized samples [*Duba et al.*, 1973], we shall limit our discussion to the present results and the data of *Shankland* [1969], *Duba* [1972], *Hughes* [1953, 1955], and *Duba and Nicholls* [1973]. All of these studies present data on highly resistive, presumably unoxidized, forsterite-rich olivine with activation energies greater than 1 eV. The results of these studies are plotted in Figure 4, and the experimental details are compiled in Table 2.

Hughes [1953] measured the σ of olivine from the same locality as the present olivine up to 1400°C in air. He reported no detectable difference in σ between the temperature increase and temperature decrease portions of the measurement cycles. In contrast, most olivines rapidly become better conductors at about 700°C in an oxidizing atmosphere; olivine from the Red Sea is apparently a notable exception [*Duba*, 1972]. *Hughes'* [1955] measurement of the σ of olivine from this

TABLE 2. Values of A_x and σ_x for σ in Single-Crystal Forsterite

Description	T Range, °C	log σ_x	A_x, eV
Hughes [1953]; Red Sea olivine (Fo 90); in air; Fig. 4, curve 5; [010]	700 to 1100 1100 to 1400	0.33 5.16	1.66 3.01
Hughes [1955]; Red Sea olivine (Fo 90); in nitrogen; Fig. 4, crosses and circles; direction unknown	1060 to 1240	5.60*	2.70
Shankland [1969]; synthetic Fo 100; in air; Fig. 4, curve 1; direction unknown	200 to 1150 1150 to 1400	-3.17 6.53	1.00 3.83
Duba [1972]; Red Sea olivine (Fo 91); in argon at 7.5 kbar; Fig. 4, curve 8; [010]	400 to 1100 1100 to 1200	-0.62 20.06(?)	1.21 7.12(?)
Duba [1972]; synthetic Fo 100; in argon at 7.5 kbar; Fig. 4, curve 9; direction unknown	750 to 1100 1100 to 1200	-0.71 21.97(?)	1.70 7.99(?)
Duba and Nicholls [1973]; San Carlos olivine (Fo 92); $f_{O_2} \sim 10^{-12}$ bar at 1200°C; Fig. 4, curve 3; [001]	800 to 950 950 to 1350	-2.33 0.81	1.07 1.82
Duba and Nicholls [1973]; San Carlos olivine (Fo 96 containing metallic Fe); $f_{O_2} \sim 10^{-12}$ bar at 1200°C; Fig. 4, curve 2; [001]	900 to 1350	2.20	2.32

*Hughes' [1955] reported σ_x yields a higher σ than is indicated by his Figure 1 or the present Figure 4.

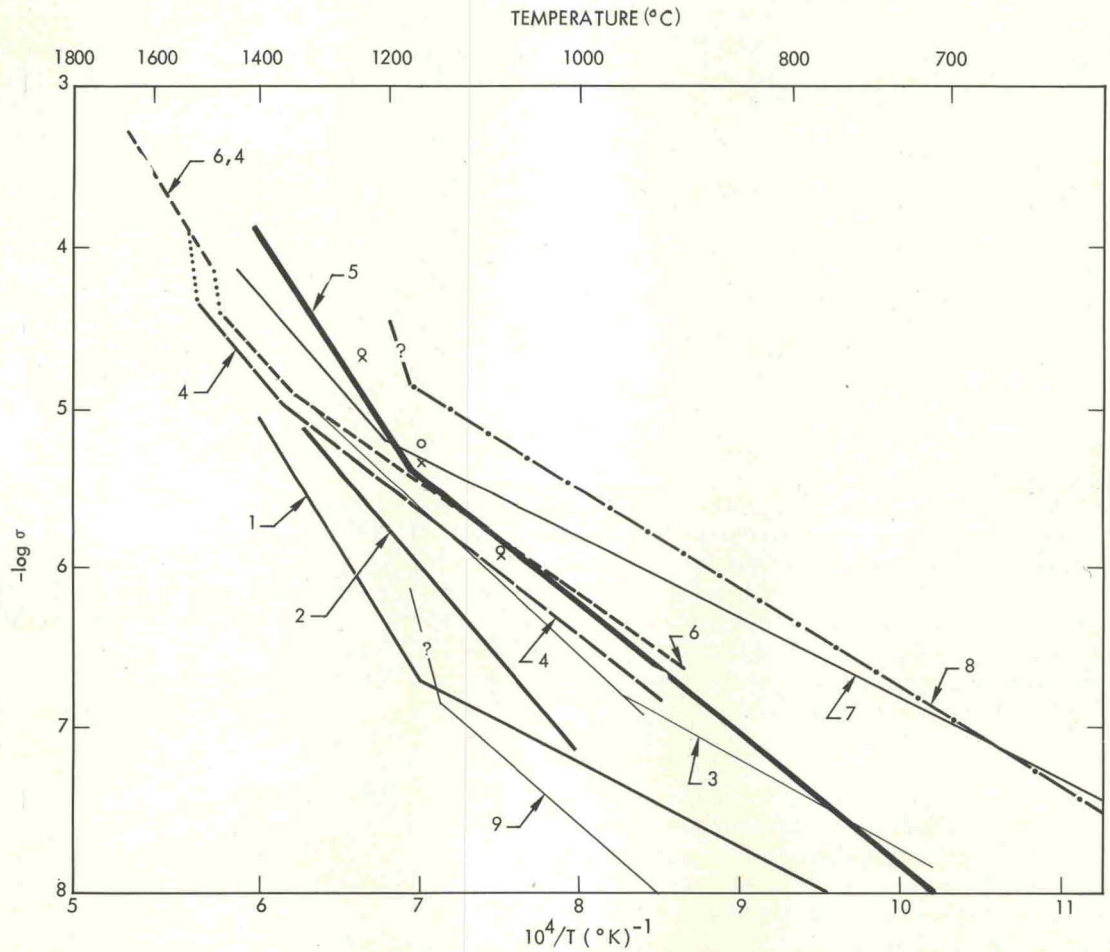

Fig. 4. Summary of σ data (Ω^{-1} cm^{-1}) for low-conductivity forsterite single crystals. The following numbers and symbols refer to data in Tables 1 and 2: curve 1, Fo 100 (~0.2 wt % Fe) [*Shankland*, 1969]; curve 2, Fo 96 [*Duba and Nicholls*, 1973]; curve 3, Fo 92 [*Duba and Nicholls*, 1973]; curve 4, cycle 1 (up), $f_{O_2} \sim 10^{-8}$ bar at 1200°C (this work); curve 5 [*Hughes*, 1953]; curve 6, cycles 1 (down), 2, and 3, $f_{O_2} = 10^{-8}$ bar at 1200°C (this work); curve 7, linear regression analysis of high pressure data (this work); curve 8, Fo 91 [*Duba*, 1972]; curve 9, Fo 100 (~0.2 wt % Mn) [*Duba*, 1972]; crosses, 8.2 kbar Fo 90 [*Hughes*, 1955]; circles, 2.5 kbar Fo 90 [*Hughes*, 1955].

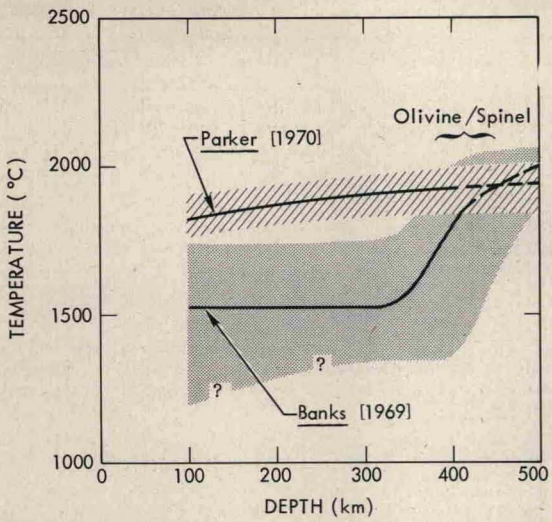

Fig. 5. Temperatures calculated for the mantle from conductivity-depth profiles and log σ_x = 4.82 (0.15), A_x = 3.13 (0.06) as reported in Table 1. Uncertainties are indicated by stippling [*Banks*, 1969] and cross-hatching [*Parker*, 1970].

locality in nitrogen to 8.2 kbar does not differ significantly from his 1953 results. However, his reported σ_x is not consistent with the data in his Figure 1, which are plotted here in Figure 4. The data of *Duba* [1972] for the Red Sea olivine to 7.5 kbar in argon are similar to those of *Hughes* [1953, 1955] and those of the present study in absolute σ below 1100°C (Figure 4), although there is some variation in A_x and σ_x as indicated in Tables 1 and 2.

The Red Sea olivine is the most resistive naturally occurring olivine [*Duba and Lilley*, 1972]. However, the conductivity of the San Carlos olivine was reduced by about 3 orders of magnitude after annealing at $f_{O_2} = 10^{-13}$ bar at about 1340°C [*Duba and Nicholls*, 1973]. This f_{O_2} is within an order of magnitude of that necessary to reduce Fe^{2+} in fayalite to metallic iron. The ensuing σ is nearly coincident with that from the Red Sea [*Duba and Nicholls*, 1973]. The reported σ for the four studies on the Red Sea olivine and the annealed San Carlos olivine differ by less than an order of magnitude above 1100°C if the very high A_x (8 eV) data [*Duba*, 1972] are excluded. We believe that value to be a result of deterioration in the Cr-Al thermocouples. The variation in σ for these olivines (Fo 90–92) reflects not only experimental uncertainties in the measurements of conductivity, temperature, and experimental atmosphere but also sample differences such as impurity contents. The latter point is illustrated by the data for the synthetic forsterite single crystals plotted in Figure 4.

The sample *Shankland* [1969] measured (curve 1) was doped with ~0.2 wt % Fe, while that of *Duba* [1972] (curve 9) contained ~0.2 wt % Mn. Also of interest is the decrease in σ of the San Carlos olivine (curve 2) after half of its iron and all of its nickel had been reduced to the metallic state [*Duba and Nicholls*, 1973] The decrease in σ is less than half an order of magnitude, but the A_x is significantly higher, indicating perhaps a change in the mechanism of conduction. The data of Figure 4 suggest that below 1400°C the σ of natural olivine is extrinsic (i.e., defect controlled), either ionic or electronic.

If the conduction mechanism is ionic, then data at the higher temperatures of this study ($T > 0.9$ of the melting temperature) may provide the activation energy for intrinsic ionic conduction [*Lidiard*, 1957]. Unfortunately, the picture is confused by the peculiar behavior noted at 1460°–1500°C, where a high activation energy is apparently superseded by a lower energy. This behavior could indicate a change in the defect structure or a chemical change in the olivine resulting from the higher f_{O_2} ($\geq 10^{-5}$ bar) at temperatures above 1460°C (Figure 3). For example, *Buening and Buseck* [1973] propose cation vacancies to explain the dependence of diffusion in olivine on f_{O_2}. Discontinuities in σ could also be due to a phase change; however, existing tnermodynamic data to 2000°K [*Robie and Waldbaum*, 1968] fail to indicate higher-order phase transitions. A reversible change in the ordering of the olivine structure (low-order transition) with increasing temperature as hypothesized by *Virgo and Hafner* [1972] could also give rise to the observed discontinuity.

Other processes that might be considered include exsolution of impurity defects at high temperatures, as proposed to explain similar behavior in BeO [*Condit and Hashimoto*, 1967], or an interaction between impurities and vacancies, which may decrease vacancy concentration at high temperatures as in doped NaCl [*Dreyfus and Nowick*, 1962]. Both mechanisms have been proposed to explain an observed decrease in activation energy at high temperatures, similar to that which is observed here. Clearly, more work needs to be done before an exact mechanism of conduction may be specified for olivine.

GEOPHYSICAL IMPLICATIONS

Figure 5 shows two temperature-depth profiles for the earth between 100 and 500 km that were calculated using σ-depth data for the earth's upper mantle [*Banks*, 1969; *Parker*, 1970], (1), and the present σ data (Figure 3) under controlled f_{O_2} at temperatures of >1500°C. Except for the addition of a lower limit to Banks' solution (indicated by the question mark in Figure 5), each profile is shown bounded by regions that reflect the temperature uncertainty resulting from the σ error and depth error that each author attributes to his determination.

The temperature-depth profiles calculated from the data of *Banks* [1969] and *Parker* [1970] are also shown in Figure 6, along with the melting curves of several relevant materials

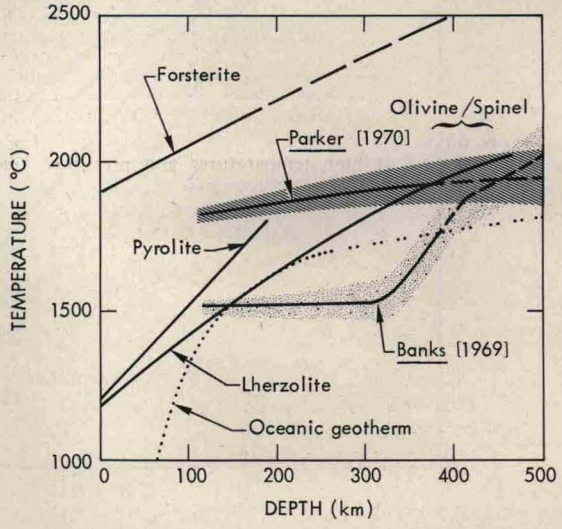

Fig. 6. Temperature-depth profile replotted from Figure 5. Uncertainty bands are based on measured pressure effect on σ (Figures 1*a*–1*c*) and σ_x and A_x values (Figure 2). Also shown are the lherzolite solidus of *Ito and Kennedy* [1967], as extended by using the Simon equation [*Griggs*, 1972], the forsterite solidus [*Davis and England*, 1964], the pyrolite solidus, and a proposed oceanic geotherm [*Ringwood*, 1966].